Neurobiology of Disease

D_2 Dopamine Receptors Colocalize Regulator of G-Protein Signaling 9-2 (RGS9-2) via the RGS9 DEP Domain, and RGS9 Knock-Out Mice Develop Dyskinesias Associated with Dopamine Pathways

Abraham Kovoor,[1,6] Petra Seyffarth,[2] Jana Ebert,[2] Sami Barghshoon,[1] Ching-Kang Chen,[3] Sigrid Schwarz,[1,2] Jeffrey D. Axelrod,[4] Benjamin N. R. Cheyette,[5] Melvin I. Simon,[1] Henry A. Lester,[1] and Johannes Schwarz[1,2]

[1]Division of Biology, California Institute of Technology, Pasadena, California 91125, [2]Department of Neurology, University of Leipzig, 04103 Leipzig, Germany, [3]Departments of Ophthalmology and Visual Sciences and Human Genetics, University of Utah, Salt Lake City, Utah 84112, [4]Department of Pathology, Stanford University School of Medicine, Stanford, California 94305, [5]Nina Ireland Laboratory of Developmental Neurobiology and Department of Psychiatry and [6]The Center for Neurobiology and Psychiatry, University of California, San Francisco, San Francisco, California 94143-0984

Regulator of G-protein signaling 9-2 (RGS9-2), a member of the RGS family of Gα GTPase accelerating proteins, is expressed specifically in the striatum, which participates in antipsychotic-induced tardive dyskinesia and in levodopa-induced dyskinesia. We report that RGS9 knock-out mice develop abnormal involuntary movements when inhibition of dopaminergic transmission is followed by activation of D_2-like dopamine receptors (DRs). These abnormal movements resemble drug-induced dyskinesia more closely than other rodent models. Recordings from striatal neurons of these mice establish that activation of D_2-like DRs abnormally inhibits glutamate-elicited currents. We show that RGS9-2, via its DEP domain (for Disheveled, EGL-10, Pleckstrin homology), colocalizes with D_2DRs when coexpressed in mammalian cells. Recordings from oocytes coexpressing D_2DR or the m2 muscarinic receptor and G-protein-gated inward rectifier potassium channels show that RGS9-2, via its DEP domain, preferentially accelerates the termination of D_2DR signals. Thus, alterations in RGS9-2 may be a key factor in the pathway leading from D_2DRs to the side effects associated with the treatment both of psychoses and Parkinson's disease.

Key words: **antipsychotic; D_2 dopamine receptor; dyskinesia; DEP domain; RGS9; striatum**

Introduction

Drugs that are effective in the treatment of psychoses (Sawa and Snyder, 2002; Freedman, 2003) and Parkinson's disease (Dauer and Przedborski, 2003) are antagonists (antipsychotics) or agonists [dopamine/L-3,4-dihydroxyphenylalanine (L-DOPA)], respectively, of G-protein-coupled D_2-like dopamine receptors (DRs). The receptors for dopamine are members of the seven transmembrane-spanning G-protein-coupled receptor (GPCR) superfamily and may be classified into two subfamilies, D_1-like (D_1 and D_5, which activate intracellular heterotrimeric G_s G-proteins) and D_2-like (D_2, D_3, and D_4, which activate heterotrimeric, pertussis toxin-sensitive G_i and G_o G-proteins) (Missale et al., 1998). Typical antipsychotics and dopamine receptor agonists also both induce motor side effects, tardive and L-DOPA-induced dyskinesia, which result from their actions on D_2-like DRs in the striatum, an important component of the basal ganglia loop that controls movement. Although the pathophysiology remains obscure, these motor side effects are strikingly similar with respect to clinical phenomenology, epidemiology, and risk factors (Rascol and Fabre, 2001).

When an activated GPCR (e.g., dopamine-bound D_2DR) encounters a trimeric G-protein, it catalyzes the exchange of GTP for GDP at the α subunit of the G-protein (Gα), leading to the dissociation of the GTP-bound Gα subunit from the G$\beta\gamma$ dimer. The activated GTP-bound Gα subunit and the freed G$\beta\gamma$ dimer regulate the activity of diverse cellular effector molecules. Signal termination is mediated by the intrinsic GTPase activity of the Gα, which hydrolyzes the bound GTP to GDP, allowing it to reassociate with the G$\beta\gamma$ dimer (Ross and Wilkie, 2000).

The GTPase activity of Gα and hence GPCR signal termination can be enhanced by members of a family of proteins called regulators of G-protein signaling (RGSs) (Berman and Gilman, 1998; De Vries et al., 2000; Ross and Wilkie, 2000). All RGS proteins have a conserved core "RGS domain" of ~120 amino acids, which is necessary and sufficient for their GTPase stimulating action. Many RGS proteins also possess additional C- and N-terminal modular protein-binding domains and motifs.

Transcripts of an RGS protein, the RGS9 splice variant

Received Jan. 15, 2004; revised Jan. 4, 2005; accepted Jan. 4, 2005.

This work was supported by grants from the Interdisziplinäres Zentrum für klinische Forschung Leipzig (TP C19), National Institutes of Health (GM-29836, GM05982, MH001750, and MH-49176), and by a National Research Service Award to A.K. (MH019552).

Correspondence should be addressed to Johannes Schwarz, Department of Neurology, University of Leipzig, 04103 Leipzig, Germany. E-mail: johannes@caltech.edu.

DOI:10.1523/JNEUROSCI.2840-04.2005

 0270-6474/05/252157-09$15.00/0

RGS9-2, are confined to the striatum (Thomas et al., 1998; Rahman et al., 1999), the brain region involved in antipsychotic-induced tardive dyskinesia and in levodopa-induced dyskinesia. Recently, Rahman et al. (2003) reported that mice with a null mutation in the RGS9 gene showed heightened locomotor responses to cocaine and related psychostimulants and that, conversely, viral-mediated overexpression of RGS9-2, but not RGS4, in rat striatum specifically reduced locomotor responses to D_2DR agonists.

The results described above prompted us to search for associations between D_2DRs and RGS9-2. The N termini of both RGS9 splice variants possess a highly conserved DEP domain (for Disheveled, EGL-10, Pleckstrin homology) (De Vries and Gist Farquhar, 1999; Druey, 2001). DEP domains are present in many key signaling proteins, but the function of this domain is not clear (Ponting and Bork, 1996). In this study, we show that the RGS9 DEP domain mediated subcellular colocalization with D_2DRs. We demonstrate that such localization has functional consequences at the cellular level and implicate a role for RGS9-2 in suppressing the extrapyramidal side effects of antipsychotic treatment and the movement disorders of Parkinson's disease.

Materials and Methods

Knock-out mice. RGS9$^{-/-}$ mice were generated as described by Chen et al. (2000). All experimental procedures complied with National Institutes of Health guidelines as approved by the Institutional Animal Care and Use Committee of the California Institute of Technology (Pasadena, CA) or the University of Leipzig (Leipzig, Germany).

Drug treatment. Reserpine, haloperidol, apomorphine, quinpirole, SKF 38393, or saline were administered intraperitoneally. Reserpine (1 mg/kg), haloperidol (5 mg/kg), or saline were administered once a day for 3 consecutive days. Behavioral testing with apomorphine (1 mg/kg), quinpirole (10 mg/kg), or SKF 38393 (10 mg/kg) was performed immediately before reserpine or haloperidol treatment and 3 d after the final injection of either drug.

Recording of locomotion and abnormal involuntary movements. Locomotion was measured using a cage rack system with infrared light beams (San Diego Instruments, San Diego, CA). Single events represented disruption of two individual light beams 10 cm apart. Data were recorded for 15 min before and after drug application. The abnormal involuntary movements (AIMs) were evaluated immediately after administration of dopamine receptor agonists. The AIMs were classified into the following four subtypes (Cenci et al., 2002; Lundblad et al., 2002): (1) axial AIMs consisting of dystonic posturing and choreiform twisting of head or neck; (2) limb movements consisting of rapid jerky movements of front limbs or hindlimbs; (3) orofacial movements including abnormal chewing, licking, grooming, etc.; and (4) abnormal locomotion comprising unsteady gait (secondary to dystonia), moving backwards, and jumping. Each of these four subtypes was scored on a severity scale from 0 to 4 (1, present during <25% of the observation time; 2, present between 25 and 50% of the observation time; 3, present between 50 and 75% of the observation time; and 4, present >75% of the observation time).

Electrophysiology in acute striatal slices. Anesthetized (halothane) mice (postnatal days 10–25) were decapitated, and brains were placed in an ice-cold artificial CSF (ACSF). Coronal slices (300 μm thick) containing striatum and globus pallidus were cut with a VT1000S vibratome (Leica, Nussloch, Germany) and stored in bubbled ACSF with kynurenic acid (1 μM) for 30 min and without kynurenic acid for at least an additional 30 min. During recordings, slices were perfused with ACSF (containing, in mM: 126 NaCl, 2.5 KCl, 2 $CaCl_2$, 1 $MgCl_2$, 1.25 NaH_2PO_4, 26 $NaHCO_3$, 25 D-glucose, pH 7.3, bubbled with 95% O_2 and 5% CO_2) at 32–33°C. More than 90% of striatal neurons are medium spiny GABAergic projection neurons. Recordings were performed on these neurons, which were identified (Axioskop infrared differential interference contrast video microscopy; Zeiss, Jena, Germany) by their small size and irregular shape (densely arborizing recurrent axon collaterals). Medium spiny neurons have two electrophysiological states, a down state with resting membrane potentials below −80 mV and no spontaneous activity and an up state with resting membrane potentials above −80 mV and high-frequency spontaneous action potentials (10–15 Hz) (Blackwell et al., 2003). In our experiments, >90% of the cells were in the down state. However, specific cell types were not identified using dye injection and immunocytochemistry. Thus, we cannot exclude that some recordings were obtained from other cell types such as GABAergic interneurons. These fast-spiking interneurons are difficult to distinguish morphologically and are also silent at rest but spike at very high frequencies (up to 200 Hz after excitation). In addition, recordings aimed at these cells are only successful in ~1 in 60 cells in striatal slice recordings (Centonze et al., 2003). Thus, it is likely that nearly all of our recordings were done in medium spiny projection neurons. These neurons have been divided into two groups based on anatomical and biochemical observations and separated into projection neurons giving rise to a direct pathway (projecting to internal globus pallidus) or an indirect pathway (projecting to external globus pallidus) (Gerfen, 1992). Recent studies have suggested that D_2-like dopamine receptors are present in both groups of medium spiny striatal neurons (Kawaguchi et al., 1990; Surmeier et al., 1996; Aizman et al., 2000; Nicola et al., 2000). Large cholinergic interneurons were excluded by size and lack of a hyperpolarization-activated cation current (I_h).

Patch electrodes were pulled (Narishige pipette puller, Tokyo, Japan) from borosilicate glass and filled with a solution containing the following (in mM): 144 K gluconate, 3 $MgCl_2$, 10 HEPES, 0.2 EGTA, pH 7.2. The resistance of the electrodes was between 3 and 9 MΩ. Series resistance was compensated 70–85% using lag values of 7–8 μs. Recordings were low-pass filtered at 2 kHz and digitized on-line at 20 kHz (DigiData 1322; pClamp9 software; Axon Instruments, Union City, CA). All drugs were dissolved in ACSF and applied using an eight-channel application system (BioMedical Instruments, Zulpich, Germany).

Antibodies. Three anti-D_2DR antibodies were used: a goat polyclonal IgG directed against the extracellular epitope in the N terminus of D_2DR, a rabbit polyclonal IgG also directed against an extracellular epitope (catalog #sc-7522 and sc-9113, respectively; Santa Cruz Biotechnology, Santa Cruz, CA), and another rabbit polyclonal IgG from Research and Diagnostics (Berkeley, CA) (catalog #AS-3526S, used in striatal immunohistochemistry). The anti-RGS9 antibody (also used in striatal immunohistochemistry) was a goat antibody from Santa Cruz Biotechnology (catalog #sc-8142). The anti-m1-muscarinic acetylcholine receptor (m1-mAChR) antibody (catalog #AMR-001) was a rabbit polyclonal from Alomone Labs (Jerusalem, Israel), and the anti-m2-mAChR antibody (catalog #AB5166) was a rat monoclonal IgG from Chemicon (Temecula, CA). All secondary antibodies were from Jackson ImmunoResearch (West Grove, PA).

Striatal immunohistochemistry. Dissected mouse brains were prefixed in 4% paraformaldehyde dissolved in PBS, pH 7.4, for 1 h at 4°C. The fixed brains were then protected in 30% sucrose in PBS for 30 min. Horizontal sections were cut at 20 μm. Before staining, sections were postfixed in 1:1 methanol/acetone for 10 min at room temperature and rehydrated in two changes of PBS (5 min each). Sections were blocked with 1% fish gelatin (Sigma-Aldrich, St. Louis, MO) in PBS at room temperature in a humid box for 1 h. Slides were incubated with 1:50 dilution of primary anti-D_2DR and anti-RGS9-2 in 1% fish gelatin in PBS at room temperature for 4 h. Sections were washed in PBS three times (5 min each wash) and were then incubated with the appropriate secondary antibody diluted in blocking solution. D_2DR was visualized using a highly cross-absorbed cyanine (Cy) 2-conjugated secondary anti-rabbit antibody, and RGS9-2 was visualized using a highly cross-absorbed Cy5-conjugated secondary anti-goat antibody (see antibody descriptions above). Sections were washed twice in PBS (10 min each wash) and mounted on cover slides using 50% glycerol in PBS.

cDNA clones and constructs. The cDNA for the D_1DR, human and the D_2DR, human, long and short forms, were provided by M. G. Caron (Duke University, Durham, NC). The RGS9-2 clone was provided by E. J. Nestler (University of Texas Southwestern Medical Center, Dallas, TX) (Rahman et al., 1999). The other cDNA clones used have been described previously (Kovoor et al., 2000). Enhanced green fluorescent protein (EGFP) cDNA was from Clontech (Palo Alto, CA). The "DEPless RGS9-2" construct was created by deleting from the full-length RGS9-2 a

segment (residues 2–220) that contained just the DEP domain. Visualization of full-length RGS9-2 and DEPless RGS9-2 distribution was facilitated by C-terminal fusion of EGFP via a flexible linker sequence: GSGGGSG. The RGS9 DEP domain construct consisted solely of the RGS9 DEP domain (residues 30–110 of RGS9) fused to the N terminus of EGFP via the spacer sequence: GDPPVAT. All constructs were engineered using standard molecular biology techniques and are shown in Figure 3.

Cell transfection and immunostaining. Cells (all lines were from American Type Culture Collection, Manassas, VA) were transfected with cDNA using Lipofectamine (Invitrogen, Carlsbad, CA) according to the manufacturer's recommendations. Cells were prepared for transfection by culturing to ~60% confluence in 30 mm poly-L-lysine-coated glass-bottom dishes (MatTek, Ashland, MA). Dishes were incubated for 2 h with 50 μg/ml poly-L-lysine (average molecular weight, 25,000; Sigma-Aldrich) in 15 mM sodium borate buffer, pH 8.4, and were then rinsed three times with sterile water. Twenty-four hours after transfection, the cells were fixed and stained in the following manner. Cells were fixed by treating with 4% paraformaldehyde (Sigma-Aldrich) freshly dissolved in PBS. Cells were made permeable by treating with PBS containing 0.2% Triton X-100 (Sigma-Aldrich) for 4 min. Nonspecific antibody binding sites were masked by incubating in blocking solution consisting of a solution 1% fish gelatin (Sigma-Aldrich) and 1% hydrolyzed casein (Sigma-Aldrich) in PBS for 30 min. Cells were then incubated with the appropriate primary antibody for 1 h at 37°C followed by incubation with the corresponding fluorophore-conjugated secondary antibody for another hour at 37°C. Antibody dilutions and incubations were performed in blocking solution. Cells were washed four times with PBS (5 min each wash) before and after every one of the above treatments. Finally, the cells were mounted by overlaying with 50% glycerol solution in PBS and stored at −20°C.

Specificity of antibodies and fluorescent signals. Control experiments to confirm specificity and validity of fluorescent signals were as follows. Primary antibody specificity was evaluated by comparing immunostaining in cells that were transfected with cDNA for the target protein with sham-transfected cells. No signal was observed in sham-transfected cells for any of the primary antibodies used. The specificity of the primary antibody signal was further confirmed by ensuring that transfected cells were not stained using normal serum from the species used to raise the antibody. Specificity of the RGS9-2 antibody was further validated by determining absence of immunostaining in striatum from RGS9 knock-out mice. Cells were also stained directly with the fluorophore-conjugated secondary antibody in the absence of the primary antibody. Insignificant fluorescent signal was noted in all of these control experiments. Thus, all the secondary antibodies used reacted only with the appropriate primary antibody and not with cellular antigens. Images of the control tissue were collected with the same settings used for the labeled tissue.

Confocal microscopy. All images were obtained using a Leica TCS laser scanning spectral inverted confocal microscope (Leica Microsystems, Bannockburn, IL) with a 40× oil immersion objective (for striatal immunohistochemistry) or a 100× oil immersion objective (all other images). EGFP and Cy2 were excited with the 488 nm line from an argon laser, Cy3 was excited with the 568 nm line from a krypton laser, and Cy2 was excited using the 633 nm line from a helium–neon laser. Emitted fluorescence was spectrally dispersed using a prism, and the spectral window for data collection by the photomultiplier tube was defined using adjustable slits. EGFP and Cy2 signals were collected using a spectral window that extended from 495 to 510 nm. Cy3 signals were collected using a spectral window that extended from 585 to 600 nm. Cy5 signals were collected using a spectral window that extended from 665 to 675 nm. The pinhole was set at ~1 Airy unit. Images were collected at a resolution of 1024 × 1024 pixels using the slowest scan-speed setting for the microscope. Only one of the fluorophores was excited (by activation of just the one corresponding laser line) during each image acquisition scan, and so the dual images from double-labeled cells were obtained sequentially instead of simultaneously. Using these conditions, we were able to ensure that there was no "bleed-through" of signal from one fluorophore into the collection window of the other in double-labeling experiments. Absence of bleed-through was confirmed by sequentially imaging cells labeled with only one of the pair of fluorophores. In these control experiments, no bleed-through was observed even as the laser power was increased 500% over that used to collect the images in the coexpression experiments.

Oocyte culture and cRNA preparation and injection. Xenopus oocyte preparation was described previously (Kovoor et al., 2000). cRNA was synthesized *in vitro* from plasmids containing the cDNA and appropriate promoters for cRNA transcription. Plasmids were linearized before cRNA synthesis, and mMessage Machine kits (Ambion, Austin, TX) were used to generate capped cRNA. cRNA was injected into oocytes at a volume of 25 nl per oocyte using a Drummond microinjector. Oocytes were maintained in a saline buffer (containing, in mM: 96 NaCl, 2 KCl, 1 $MgCl_2$, 1 $CaCl_2$, and 5 HEPES, pH 7.5) solution supplemented with sodium pyruvate (2.5 mM) (Sigma-Aldrich) and gentamycin (50 μg/ml) (Sigma-Aldrich).

Oocyte electrophysiology. Two-electrode voltage-clamp experiments were performed 36–72 h after cRNA injection. Membrane potential was clamped at −80 mV using a GeneClamp 500 amplifier and pClamp 6 software (Axon Instruments). A valve system controlled by the data acquisition software, pClamp 6, was used to control solution changes and to minimize wash-in and wash-out times. Electrodes were filled with 3 M KCl and had resistances of 0.5–1.5 MΩ. To reveal currents through the inwardly rectifying G-protein-gated inward rectifier potassium (GIRK) channels, recordings were performed in oocyte saline buffer with elevated (16 mM) KCl concentration (other components, in mM: 82 NaCl, 1 $MgCl_2$, 1 $CaCl_2$, and 5 HEPES, pH 7.5). Kinetic analysis and curve fitting were performed using pClamp 6 software. Exponentials were fit to the activation and deactivation phases of the GIRK currents. Cursors were positioned at points on the activation and deactivation curves that corresponded to 20 and 80% of the maximum equilibrium responses, and the exponentials were fitted to the portions of the current trace between these two points.

Results

RGS9-2 attenuates motor behavior related to upregulated D_2DR

We treated RGS9 knock-out mice and wild-type mice with reserpine, which depletes dopamine from nerve terminals, or with the antipsychotic haloperidol, a specific antagonist of D_2-like DRs (see Materials and Methods). Both reserpine and haloperidol treatments can selectively produce supersensitivity of striatal D_2-like DRs (LaHoste and Marshall, 1994). We observed no obvious behavioral differences between drug-naive RGS9 knock-out animals and wild-type littermates. Reserpine treatment for 3 d (see Materials and Methods) produced a comparable loss of spontaneous locomotion in both groups (data not shown). However, after reserpine or haloperidol treatment, dopaminergic agonists (quinpirole, selective agonist of D_2-like DRs or apomorphine, nonselective agonist of D_1- and D_2-like DRs) produced severe AIMs (Fig. 1*A*,*C*) (see also http://orphanin.caltech.edu/~lester/world/Videos%20for%20RGS9%20JNS%20paper/ for video clips) only in the RGS9-deficient mice (AIM score, >4; see Materials and Methods). Gait alterations included excessive sideward and backward motions. These animals also had difficulties maintaining an upright posture and repeatedly hit the cage wall. There were frequent rapid jerky movements, predominantly of hindlimbs. Most animals also showed an excessively bent trunk resembling dystonia. Apomorphine and quinpirole also produced a greater increase in locomotion after reserpine in the RGS9 knock-out mice (Fig. 1*B*). The genetic ablation of RGS9 did not affect D_1 dopamine receptor-related behavior: the D_1DR agonist SKF 38393, after reserpine or haloperidol, elicited comparable mild orofacial AIMs and locomotion in both wild-type and knock-out animals (Fig. 1*A*–*C*). These data suggest that the

observed AIMs result from the perturbation of a D_2-like DR-specific cellular pathway.

Administration of dopaminergic agonists before reserpine or haloperidol treatment produced few AIMs (mean AIM, <1 in both groups) in either wild-type or RGS9-null animals. In accordance with previous reports (LaHoste and Marshall, 1994; LaHoste et al., 2000), relevant AIMs were not observed in either set of mice pretreated with vehicle injections for 3 d and subsequently challenged with quinpirole (10 mg/kg).

The relatively short duration of reserpine or haloperidol treatment (3 d) may explain why significant increases in locomotion after reserpine or after haloperidol only occurred in response to apomorphine and only in RGS9 knock-out mice.

Previously, double-labeling *in situ* hybridization experiments suggested that RGS9-2 transcripts are expressed in those striatal neurons that might also express D_2DR (Rahman et al., 2003). Immunostains of striatal sections confirmed that there was a significant degree of overlap of D_2DR and RGS9-2 protein expression in the striatum (Fig. 1*D*).

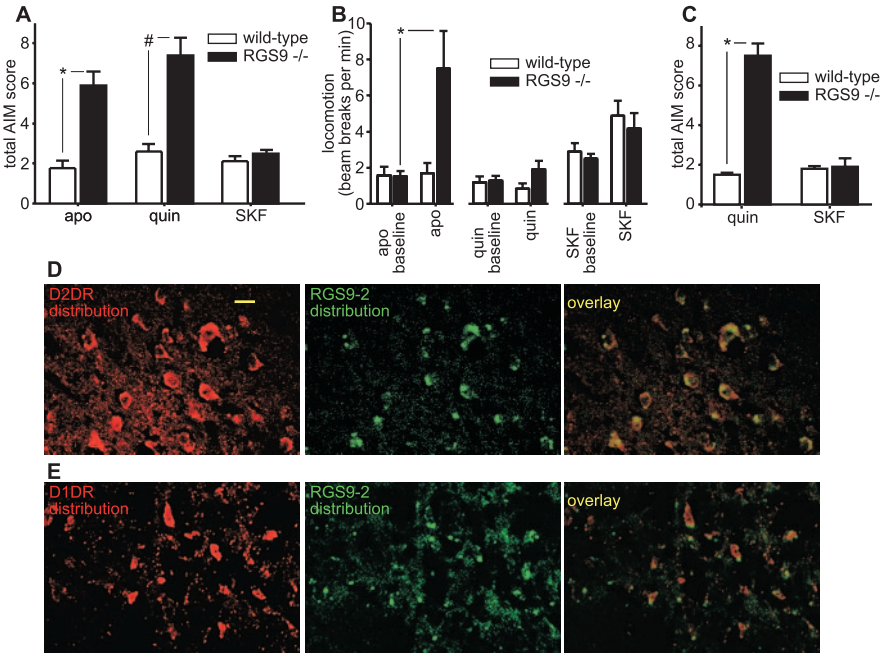

Figure 1. Behavioral effects of dopamine agonists in reserpinized or haloperidol-treated mice and distribution of D_2DR and RGS9-2 in wild-type striatal neurons. Mice were injected once per day for 3 d with reserpine or haloperidol (see Materials and Methods). Three days after recovery, the mice were injected with dopaminergic agonists. Open bars represent wild-type mice, and filled bars represent RGS9-deficient mice. ***A***, Quantification of abnormal involuntary movements in reserpinized mice after apomorphine (apo; $n = 13$ and 18 in wild-type and knock-out, respectively), quinpirole (quin; $n = 10, 14$), or SKF 38393 (SKF; $n = 9, 8$) injection (# and * indicate significant differences between genotypes; $p < 0.01$; Wilcoxon rank test). ***B***, Locomotion measured (for 15 min) in the reserpinized mice (from ***A***) immediately before (baseline) and after apo, quin, or SKF injection (*$p <$ 0.01; *t* test). ***C***, Quantification of AIM in haloperidol-treated mice after quin or SKF injection ($n = 10$; *$p < 0.01$; Wilcoxon rank test). ***D***, D_2DR distribution (red; left), RGS9-2 distribution (green; middle), and their overlay (right) in a striatal section. The left and middle panels represent sequential confocal scans of the same field. ***E***, D_1DR distribution (red; left), RGS9-2 distribution (green; middle), and their overlay (right) in a striatal section. The left and middle panels represent sequential confocal scans of the same field. Scale bar: (in ***D***) ***D***, ***E***, 10 μm. Error bars represent SEM.

A role for RGS9-2 in cellular signaling of D_2-like DR *in vivo* and implications for synaptic modulation

Previously, we helped to show that D_2DR activation produced a significantly greater inhibition of forskolin-stimulated adenylyl cyclase activity in striatal extracts from RGS9 knock-out animals compared with their wild-type littermate controls (Rahman et al., 2003). The striatal medium spiny neurons that express D_2-class dopamine receptors and RGS9-2 receive excitatory glutamatergic inputs from the cortex in addition to the dopaminergic inputs from the substantia nigra (Gerfen, 1992). Therefore, we investigated whether the activation of D_2-like DRs could modulate glutamate-elicited conductances in these cells. Application of glutamate (100 μM) to voltage-clamped medium spiny neurons in slice preparations from either wild-type or RGS9-null mice activated robust inward currents (Fig. 2*A*,*B*). These currents desensitized partially during a 6 s glutamate application (Fig. 2*A*,*B*). The desensitization was transient, and the response recovered after >3 min of glutamate-free wash. Coapplication of 1–100 μM quinpirole, a selective agonist of D_2-like DRs, significantly inhibited the peak amplitude of the glutamate-elicited response in RGS9 null neurons, whereas there was no significant reduction by quinpirole in wild-type cells (Fig. 2*A*,*B*). Although quinpirole concentrations >10 μM may affect targets in addition to D_2DR, it is notable that statistically significant inhibition of glutamate-elicited currents in the knock-out animals were observed both at 1 and 10 μM quinpirole (Fig. 2*B*). The fraction of RGS9-null cells that showed >25% inhibition of glutamate (100 μM)-induced currents was 0.5 at 1 μM and increased to 0.67 at 10 μM and 1.0 at 100 μM. In contrast, the fraction of wild-type cells in which the glutamate-elicited currents were inhibited >25% was 0.22 (1 and 10 μM quinpirole) or 0.44 (100 μM quinpirole). Application of quinpirole alone produced no changes in membrane conductance of either wild-type or RGS9-null neurons. We used 100 μM quinpirole to study effects on NMDA- or AMPA-induced currents because we detected the most striking differences between genotypes at this concentration. NMDA receptors accounted for the component of glutamate-evoked currents modulated by quinpirole in the RGS9-null cells, because 100 μM quinpirole significantly inhibited NMDA-elicited (100 μM) but not AMPA-elicited (10 μM) currents (Fig. 2*C*). Finally, the inhibitory effects of quinpirole were blocked by the specific D_2-like DR antagonist sulpiride, confirming that they were mediated via D_2-like DRs.

The abnormal inhibition of glutamate-elicited currents by D_2-like DRs in the absence of RGS9 was not a result of increased expression of glutamate receptors, because the amplitude of the glutamate response was not increased in RGS9-null neurons (Fig. 2). These data suggest that in wild-type neurons, RGS9-2 blocks D_2-like DR-mediated modulation of conductances elicited by activation of NMDA receptors. Because it seemed unlikely that this effect arises solely from the GTPase-enhancing activity of RGS9-2, we explored other functional associations between RGS9-2 and D_2DRs, the most abundantly expressed D_2-like DRs.

D_2DR, RGS9-2 colocalization

RGS9-2 and D_2DRs were expressed *in vitro* in Chinese hamster ovary (CHO) cells and visualized using confocal microscopy. The D_2DR expression was visualized by immunostaining CHO cells with the anti-D_2DR antibody after they were first made perme-

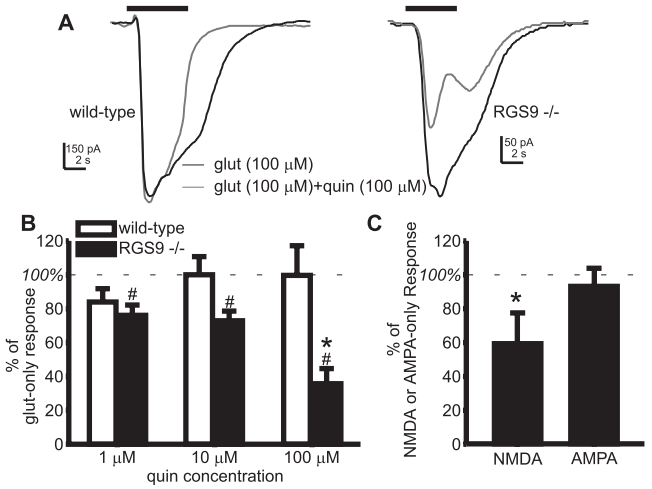

Figure 2. Effects of the D_2-like DR agonist quinpirole (quin) on excitatory currents elicited from medium spiny striatal neurons. ***A***, Representative traces of currents evoked from the same voltage-clamped (−70 mV) striatal medium spiny neuron in response to glutamate (glut; 100 μM; black trace) or glutamate and quinpirole (glut, 100 μM plus quin, 100 μM; gray trace). Left, Wild-type neuron; right, RGS9-deficient neuron. Black bars above the traces represent drug application. ***B***, Glut- and quin-elicited current expressed as a percentage of the current evoked by glut alone (100 μM) from wild-type (open bars) and RGS9-deficient (filled black bars) neurons. The mean ± SEM peak current amplitudes in picoamperes for wild-type cells were: glut alone, 607 ± 81 ($n = 9$); glut plus 1 μM quin, 488 ± 63 ($n = 9$); glut plus 10 μM quin, 574 ± 85 ($n = 9$); glut plus 100 μM quin, 602 ± 108 ($n = 9$); and for RGS9-deficient cells: glut alone, 316 ± 71 ($n = 9$); glut plus 1 μM quin, 257 ± 54 ($n = 8$); glut plus 10 μM quin, 250 ± 52 ($n = 6$); glut plus 100 μM quin, 155 ± 52 ($n = 8$). ***C***, Current evoked by NMDA (100 μM; $n = 7$) or AMPA (10 μM; $n = 5$) in the presence of quin (100 μM) expressed as a percentage of the current evoked, respectively, by NMDA or AMPA alone from RGS9-deficient neurons. The mean ± SEM peak current amplitudes in picoamperes were as follows: NMDA alone, 442 ± 106; NMDA plus quin, 230 ± 87; AMPA alone, 266 ± 66; AMPA plus quin, 247 ± 28. The # symbol indicates that the quinpirole-sensitive fraction of the current differs significantly from zero. p values using a paired t test are 0.03, 0.04, and 0.008 at 1, 10, and 100 μM quinpirole, respectively. The corresponding p values for the wild-type animals were 0.07, 0.8, and 0.9, respectively. The asterisk indicates that the quinpirole-sensitive fraction of the current differs significantly from the corresponding wild-type sample. $p < 0.01$; ANOVA. Error bars represent SEM.

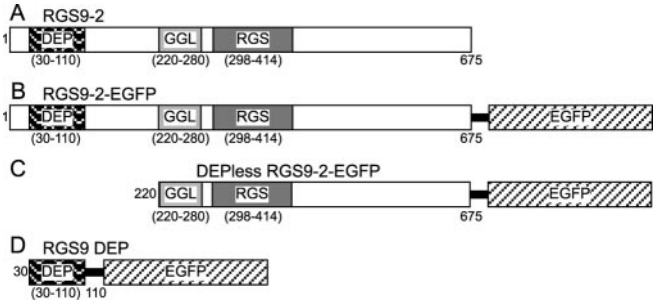

Figure 3. Schematic representation (N to C terminus) of the RGS9 constructs. The numbers in parentheses indicate the position of each indicated domain in the original wild-type protein. The numbers at either end of the open boxes represent the span of the wild-type protein used in each construct. ***A***, Schematic representation and domain composition of full-length wild-type RGS9-2. ***B***, The full-length RGS9-2–EGFP fusion construct. The black bar between the RGS9-2 and EGFP represents a flexible spacer/linker with the following sequence: GSGGGSG. ***C***, The DEPless RGS9-2–EGFP fusion construct in which the N-terminal region of RGS9 containing the DEP domain was deleted but was otherwise identical to the full-length RGS9-2–EGFP fusion. ***D***, The RGS9 DEP domain fusion construct. The linker represented by the black bar has the following sequence: GDPPVAT. GGL, G-protein γ-subunit-like domain.

able using the detergent Triton X-100 (see Materials and Methods). Using this same protocol, identical staining patterns were obtained using three separate antibodies that were directed against different intracellular and extracellular epitopes within D_2DR. No D_2DR immunostain was observed in dishes not transfected with D_2DR cDNA.

To observe RGS9 distribution, we used an RGS9-2 fusion construct, RGS9-2–EGFP, in which the EGFP was attached to the C terminus of the full-length striatally expressed RGS9 isoform, RGS9-2 (Fig. 3) (see Materials and Methods).

The D_2DR expression pattern in CHO cells (Fig. 4*A*) was consistent with previous studies showing that ≥80% of the D_2DR expressed in several cell types, including human embryonic kidney (HEK) 293T, COS-7, and HeLa, resides within intracellular compartments (Prou et al., 2001). It was also consistent with our observations in striatal neurons in which D_2DR is in extranuclear accumulations (compare Figs. 1*D*, 4*A*). In CHO cells transfected solely with the RGS9-2 cDNA, the RGS9-2 protein was distributed uniformly throughout the cytoplasm (Fig. 4*B*). However, when CHO cells were transfected with cDNA for both D_2DR and the RGS9-2, we found that the expression pattern of RGS9-2 was dramatically altered and was now identical to the patchy distribution pattern seen for D_2DR (Fig. 4*C*).

Targeting of DEP domains to D_2DR

To identify the molecular domains required for targeting RGS9-2 to D_2DR, we created two constructs, DEPless RGS9-2 and the RGS9 DEP domain (Fig. 3) (see Materials and Methods). When expressed alone, both protein constructs were distributed uniformly throughout the cytoplasm (Fig. 4*F*,*H*). Coexpression with D_2DR altered the distribution: the RGS9 DEP domain was targeted to the distinctive, cytoplasmic compartments expressing D_2DR, whereas the distribution pattern of DEPless RGS9-2 was unaffected (Fig. 4*G*,*I*, respectively), suggesting that the DEP domain is both necessary and sufficient for targeting RGS9-2 to D_2DR. The patterns shown here for CHO cells were reproduced in experiments with HEK 293T and NIH3T3 cell lines (data not shown).

All results shown are with the D_2short (D_2s) DR, but identical results were obtained with D_2long DR, which contains 29 additional amino acids in the third cytoplasmic loop (Missale et al., 1998), suggesting that this loop plays no important role in the association with DEP domains. Likewise, a mutant D_2sDR lacking the cytoplasmic-tail (1) had wild-type like subcellular distribution and (2) was able to colocalize the RGS9 DEP domain (data not shown).

DEP domains target to plasma membrane-localized D_2DR

In most of the cell lines tested, the fluorescence of the large pool of intracellular D_2DR overwhelmed any signal from plasma membrane-associated molecules. Do RGS9-2 and D_2DR associate at the plasma membrane, where RGS9-2 presumably functions? We transfected undifferentiated rat pheochromocytoma 12 (PC12) cells with D_2DR cDNA using a lipid-mediated transfection protocol. Under these conditions, we found that D_2DR was expressed primarily in the plasma membrane (Fig. 4*J*) when these cells were examined 24–36 h after transfection. RGS9-2 and DEPless RGS9-2, when expressed alone in these cells, appeared uniformly through the cytosol (Fig. 4*K*,*M*). Coexpression of D_2DR with full-length RGS9-2, but not with DEPless RGS9-2, resulted in an enriched RGS9-2 signal at the plasma membrane (compare Figs. 4*L*, green panel; 3*K*,*M*,*N*, green panels).

We tested the effect of D_2DR agonists on the colocalization of D_2DR and DEP domain-containing constructs. Cells were incubated with dopamine (1 μM), apomorphine (1 μM), or quinpirole (1 μM) for periods ranging from 5 min to 24 h. These D_2DR agonists did not affect the cellular distribution of D_2DR or the association between D_2DR and DEP domains in PC12 cells or CHO cells (data not shown).

Functional effects of D_2DR–RGS9-2 colocalization

RGS9-2 did not colocalize detectably to any other GPCRs that were screened. These included (1) the G_q-coupled m1-mAChR, the cellular expression pattern of which matches that of D_2DR (Fig. 5*A*,*B*), (2) the G_s-coupled D_1 dopamine receptor (Fig. 5*C*,*D*), and (3) the G_i- and G_o-coupled m2-mAChR (Fig. 5*E*,*F*).

We used the *Xenopus* oocyte system to suggest a functional consequence for this specific DEP domain-dependent localization of RGS9-2 to D_2DR. It is appropriate to assay for the GTPase-enhancing property of RGS proteins by measuring the accelerated deactivation of coexpressed GIRK channels (Doupnik et al., 1997; Kovoor et al., 2000; Rahman et al., 2003). Figure 5, *G* and *H*, depicts representative normalized traces of deactivation waveforms for dopamine-evoked (100 nM; red trace) and acetylcholine-evoked (100 nM; black trace) GIRK currents recorded from the oocyte group expressing the appropriate receptor and either RGS9-2 (Fig. 5*G*) or DEPless RGS9-2 (Fig. 5*H*). For several RGSs including RGS9, deletions N-terminal to the RGS domain enhanced the intrinsic GTPase-enhancing function of the RGS protein (Fig. 5*H*,*I*) (Kovoor et al., 2000; A. Kovoor and H. A. Lester, unpublished observations). Thus, the functional consequence of the failure of DEPless RGS9-2 to colocalize with D_2DR would be obscured by the increased intrinsic activity of the DEPless construct, vitiating direct comparisons between the action of RGS9-2 and DEPless RGS9-2 on the D_2DR response. Instead, comparisons were made between signaling by D_2DR and m2-mAChR, because the latter GPCR displays no RGS9-2 colocalization (Fig. 5*E*,*F*).

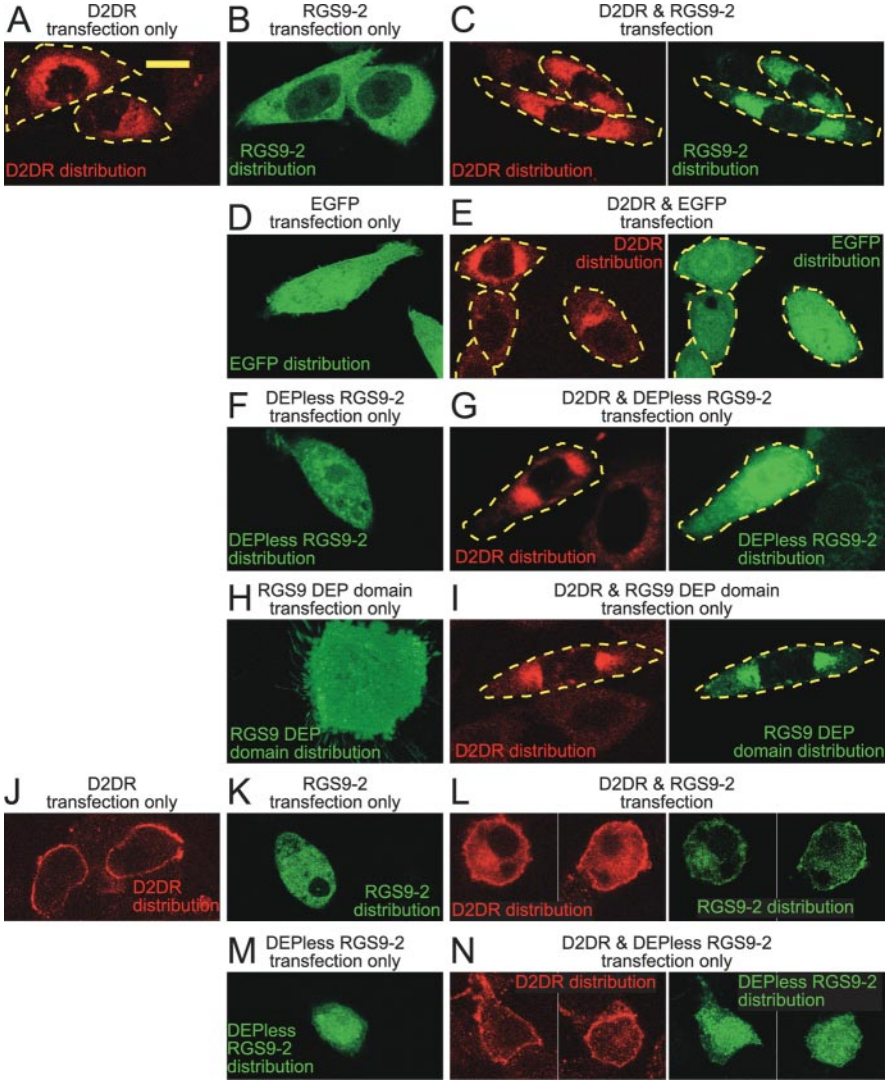

Figure 4. Distribution of D_2DR and RGS9-2 in transfected CHO and PC12 cells. D_2DR distribution is depicted in red, whereas RGS9-2 constructs and EGFP are shown in green. ***A***, D_2DR distribution in CHO cells that were transfected with cDNA for D_2DR alone. ***B***, RGS9-2 distribution in CHO cells that were transfected with cDNA for the RGS9-2 alone. ***C***, D_2DR distribution (red; left) and RGS9-2 distribution (green; right) in CHO cells transfected with cDNA for both D_2DR and the RGS9-2. ***D***, EGFP distribution in CHO cells transfected with cDNA for EGFP alone. ***E***, D_2DR distribution (red; left) and EGFP distribution (green; right) in CHO cells transfected with cDNA for both D_2DR and EGFP. ***F***, DEPless RGS9-2 distribution in CHO cells that were transfected with cDNA for DEPless RGS9-2. ***G***, D_2DR distribution (red; left) and DEPless RGS9-2 distribution (green; right) in CHO cells transfected with cDNA for both D_2DR and DEPless RGS9-2. ***H***, RGS9 DEP domain distribution in CHO cells that were transfected with cDNA for the RGS9 DEP domain alone. ***I***, D_2DR distribution (red; left) and RGS9 DEP domain distribution (green; right) in CHO cells transfected with cDNA for both D_2DR and RGS9 DEP domain. ***J***, D_2DR distribution in PC12 cells that were transfected with cDNA for D_2DR alone. ***K***, RGS9-2 distribution in PC12 cells that were transfected with cDNA for the RGS9-2 fusion protein alone. ***L***, D_2DR distribution (red; left) and RGS9-2 distribution (green; right) in PC12 cells transfected with cDNA for both D_2DR and the RGS9-2 fusion construct. ***M***, DEPless RGS9-2 distribution in PC12 cells that were transfected with cDNA for DEPless RGS9-2. ***N***, D_2DR distribution (red; left) and DEPless RGS9-2 distribution (green; right) in PC12 cells transfected with cDNA for both D_2DR and DEPless RGS9-2. The left and right pictures, respectively, in panels ***C***, ***E***, ***G***, ***I***, ***L***, and ***N*** represent confocal scans of the same field. Outlines of cells in which the specific fluorescent signal does not extend to the cell boundary are marked out with a yellow dashed line. Each CHO cell image is representative of the distribution pattern in >90% of cells in at least five observed fields, each containing >50 cells transfected with the relevant constructs. For PC12 cells, each image is representative of the distribution pattern observed in >90% of cells from at least 20 observed fields, each containing at least one cell transfected with the relevant constructs. Scale bar: (in ***A***) ***A***–***N***, 5 μm.

Although the intrinsic deactivation rates (in the absence of RGS9) of the D_2DR and m2-mAChR response were similar, the RGS9-2-mediated acceleration of the deactivation rate was significantly greater for the D_2DR response (Fig. 5*G*,*I*). DEPless RGS9-2 also accelerated the deactivation kinetics of both the D_2DR-elicited and m2-mAChR-elicited GIRK response (Fig. 5*H*,*I*). However, in contrast to observations with full-length RGS9-2, the acceleration of the deactivation rates of the D_2DR response was not significantly different from the deactivation rate for the m2-mAChR response (Fig. 5*I*). Thus, full-length RGS9-2 preferentially accelerates the deactivation of D_2DR-elicited responses, whereas DEPless RGS9-2 does not. To prevent several classes of artifacts, the ratios of receptor and GIRK cRNA injected were chosen so that (1) the

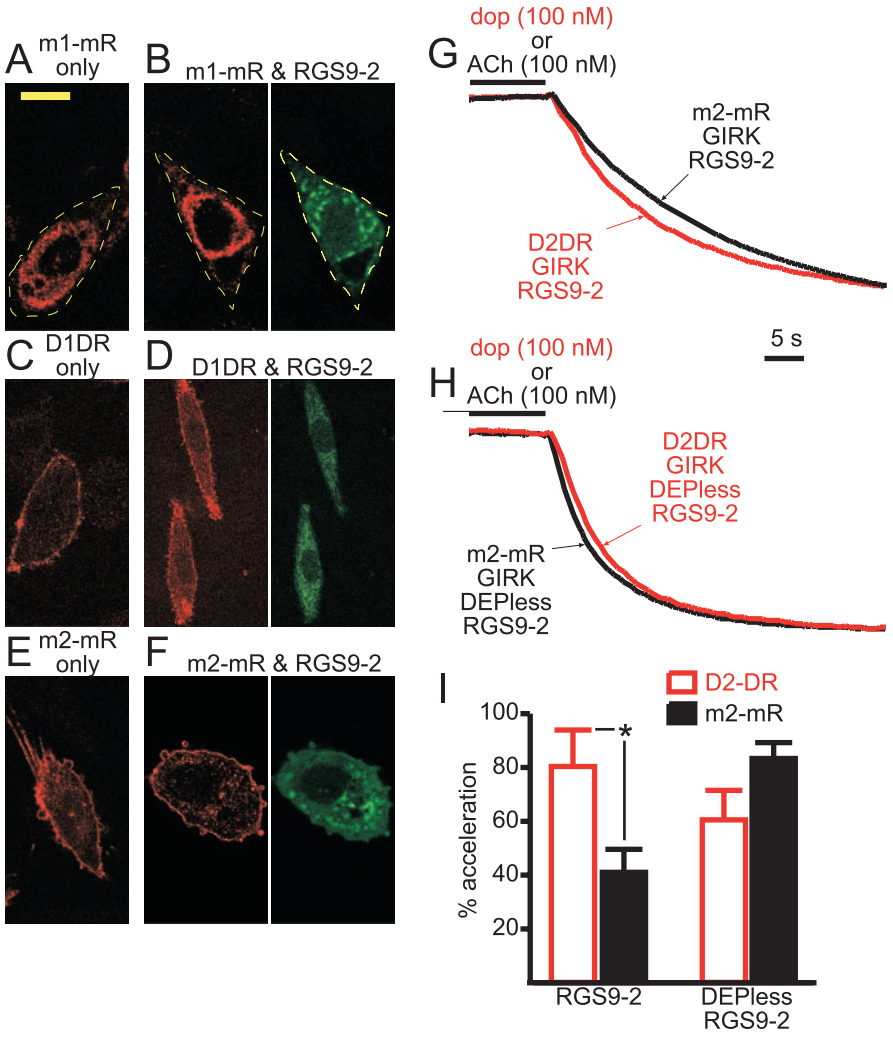

Figure 5. Distribution of m1-mAChR, D_1DR, m2-mAChR, and RGS9-2 in transfected CHO cells and effect of RGS9-2 and DEPless RGS9-2 on the deactivation kinetics of D_2DR- or m2-mAChR-elicited GIRK currents in *Xenopus* oocytes. ***A***, m1-mAChR (labeled m1-mR) distribution in cells that were transfected with cDNA for D_2DR alone. ***B***, m1-mR distribution (red; left) and RGS9-2 distribution (green; right) in cells transfected with cDNA for both m1-mR and RGS9-2. ***C***, D_1DR distribution in cells that were transfected with cDNA for D_1DR alone. ***D***, D_1DR distribution (red; left) and RGS9-2 distribution (green; right) in cells transfected with cDNA for both D_1DR and the RGS9-2. ***E***, m2-mAChR (labeled m2-mR) distribution in cells that were transfected with cDNA for D_2DR alone. ***F***, m2-mR distribution (red; left) and RGS9-2 distribution (green; right) in cells transfected with cDNA for both D_2DR and RGS9-2. The left and right pictures, respectively, in ***B***, ***D***, and ***F*** represent confocal scans of the same field. Outlines of cells in which the fluorescence does not extend to the cell boundary are marked out with a yellow dashed line. Each image is representative of the distribution pattern in >90% of cells in at least five observed fields, each containing >50 cells transfected with the relevant constructs. Scale bar: (in ***A***) ***A–F***, 5 μm. In the *Xenopus* oocyte experiments, control oocytes were injected with cRNA for m2-mR, GIRK1, and GIRK2 or with cRNA for D_2DR, GIRK1, and GIRK2. Some oocytes in each of the control groups were also injected with cRNA for either RGS9-2 or for the DEPless RGS9-2. ***G***, ***H***, Representative normalized traces of deactivation waveforms for dopamine-evoked (dop; D_2DR agonist; 100 nM; red trace) and acetylcholine-evoked (m2-mR agonist; 100 nM; black trace) GIRK currents recorded from the oocyte group expressing the appropriate receptor and either RGS9-2 (***G***) or DEPless RGS9-2 (***H***). The horizontal bar above the traces represents either dopamine or acetylcholine application. ***I***, Deactivation rate constants, k_{off} ($1/\tau_{deactivation}$), were from exponential fits of the deactivation phase of the GIRK currents. For each receptor, acceleration of deactivation by RGS9-2 was calculated as follows: (individual values for k_{off} in the oocytes injected with RGS9-2 cRNA)/(mean k_{off} in the corresponding control group lacking RGS9-2). Acceleration of deactivation by DEPless RGS9-2 was calculated similarly. All bars are means ± SEM from the same oocyte donor (red open bar, D_2DR response; black open bar, m2-mR response; * indicates significant difference; $p < 0.05$; Student's *t* test). In the experiment measuring RGS9-2-mediated acceleration of the deactivation kinetics, the mean ± SEM k_{off} values in seconds $^{-1}$ for the different oocyte groups were as follows: D_2DR, 0.057 ± 0.006 ($n = 4$); D_2DR plus RGS9-2, 0.102 ± 0.007 ($n = 5$); m2-mR, 0.055 ± 0.003 ($n = 5$); m2-mR plus RGS9-2, 0.078 ± 0.004 ($n = 5$), and the mean ± SEM steady-state current amplitudes in nanoamperes were: D_2DR, 1094 ± 284; D_2DR plus RGS9-2, 1125 ± 128; m2-mR, 1460 ± 153; m2-mR plus RGS9-2, 1416 ± 102. In the experiment measuring DEPless RGS9-2-mediated acceleration, the mean ± SEM k_{off} values in seconds $^{-1}$ were as follows: D_2DR, 0.131 ± 0.021 ($n = 5$); D_2DR plus DEPless RGS9-2, 0.211 ± 0.014 ($n = 8$); m2-mR, 0.123 ± 0.008 ($n = 12$); m2-mR plus DEPless RGS9-2, 0.225 ± 0.007 ($n = 12$), and the mean ± SEM steady-state current amplitudes in nanoamperes were: D_2DR, 618 ± 43; D_2DR plus DEPless RGS9-2, 943 ± 158; m2-mR, 964 ± 90; m2-mR plus DEPless RGS9-2, 953 ± 92. Error bars represent SEM.

level of expressed receptor and not of GIRK channel was limiting, (2) the GIRK responses elicited by m2-mAChR and D_2DR were comparable, and (3) all kinetic measurements were well resolved by our changes.

Discussion

DEP domain GPCR interactions are specific

The observations that the EGFP tag was not colocalized to D_2DR and that its distribution was not altered by coexpressed D_2DR argue for a specific interaction between D_2DR and EGFP-tagged RGS9-2 (Fig. 4*D*,*E*). In addition, an RGS9-2 construct lacking the DEP domain did not colocalize with D_2DR. In fact, the RGS9 DEP domain is both necessary and sufficient for targeting RGS9-2 to the cellular regions expressing D_2DR (Fig. 4*F–I*). Also, RGS9-2 (Fig. 5) and the RGS9 DEP domain (data not shown) did not colocalize with m1-mAChR (Fig. 5*A*,*B*), which had an expression pattern comparable with that of D_2DR in CHO cells or with D_1DR (Fig. 5*C*,*D*). Thus, overexpression of a GPCR did not guarantee association. Finally, a construct containing a mutated DEP domain (F115S; data not shown) failed to relocalize to coexpressed D_2DR.

These data point to a specific targeting of RGS9-2 to D_2DR and exclude coincidental colocalization, because the distribution of full-length RGS9-2 and the DEP domain was altered by D_2DR coexpression. After D_2DR coexpression, DEP domain-containing constructs were relocated to the compartment expressing D_2DR (i.e., to the plasma membrane in PC12 cells and to the D_2DR-expressing cytoplasmic compartments in other cell types). If the interaction between RGS9-2 and D_2DR occurs via a third protein, this additional protein is expressed in all cell types that were examined.

GPCR, RGS proteins, and signal specificity

This study suggests how RGS regulation can be targeted to a specific G-protein-coupled receptor pathway. The agonist-independent, DEP domain-dependent colocalization positions RGS9-2 close to the D_2DR-coupled Gα subunits. After Gα subunits are released by activated D_2DRs, the proximity of RGS9-2 to D_2DR allows RGS9-2 to readily interact with and inactivate these nearby G-protein subunits. The functional effects of such colocalization become even more prominent in neurons, which have a more complex morphology than *Xenopus* oocytes and have

specialized regions such as axon terminals, initial segments, and dendrites. Our model provides a molecular explanation for two recently published studies. In one study, viral-mediated overexpression of RGS9-2, but not RGS4, in rat ventral striatum, reduced locomotor responses specifically to D_2DR agonists (Rahman et al., 2003). In another study, RGS9 reduced D_2DR modulation of $Ca_v2.2$ channels but did not alter m2-muscarinic receptor modulation of $Ca_v2.2$ currents in the same neuron (Cabrera-Vera et al., 2004).

Implications for synaptic modulation by D_2DRs

Our use of GIRK channels in the *Xenopus* oocyte experiments (Fig. 5) does not suggest that they are effector molecules for D_2DRs in the striatum. In fact, the effector molecules important in striatal D_2-like DR signaling pathways have not been identified (Nicola et al., 2000). However, D_2-like DRs in the striatum signal via heterotrimeric G-proteins and GIRK channels are activated by these same G-proteins (Dascal, 2001). Previously, we have shown that the activation of coexpressed GIRK channels is a sensitive measure of the physiologically relevant activation of G-proteins and of RGS function (Kovoor et al., 2000). Similarly, in this study, these channels were used to show that the DEP domain-mediated localization of RGS9 to D_2DRs can have functional consequences for G-protein-mediated D_2DR signaling.

Both excitatory glutamatergic inputs from the cortex and dopaminergic inputs from the substantia nigra make synaptic contacts with the medium spiny neuron (Gerfen, 1992), which express glutamate receptor subunits and dopamine receptors. Our data clearly demonstrate that RGS9 is an important regulator of the neuronal pathways that modulate the membrane conductances elicited by NMDA-type glutamate receptor activation. This modulation may be important in drug-induced dyskinesia, because recent study in primates indicates that levodopa-induced dyskinesias can be modulated via NMDA and AMPA receptors. Antagonists of AMPA receptors reduce D_1DR agonist-induced dyskinesias, and antagonists of NMDA receptors reduce D_2DR agonist-induced dyskinesia (Bibbiani et al., 2004). In addition, hemiparkinsonian rats chronically treated with levodopa also show abnormal phosphorylation of NMDA receptors (Dunah et al., 2000). The present experiments also provide the first physiologically relevant description of a cellular function for an RGS protein in the brain.

Because voltage-clamp recordings in neurons can be limited by inadequate space clamp, it is possible that glutamate application strongly depolarized regions of the neurons, locally activating voltage-dependent channels. Conceivably then, it is not the NMDA receptors but these secondary conductances that are inhibited by quinpirole in striatal slices from the RGS9 knock-out animals, and NMDA and AMPA receptors are differentially localized to the extent that they activate distinct secondary conductance. Thus, although our data indicate that the striatal signal transduction pathways modulated by RGS9-2 are closely associated with NMDA but not AMPA receptors, a direct interaction between the dopaminergic and glutamatergic receptors cannot yet be claimed.

Pharmacological tests do not distinguish conclusively between the D_2DRs and the other D_2-class DRs (D_3 and D_4). Drug-induced dyskinesias are elicited by agonists and antagonists acting on all members of the D_2 class of dopamine receptors, and the contributions of D_2 versus D_3 versus D_4 receptors for the pathogenesis of this condition is not clear. Therefore, discrimination of the effect of lack of RGS9 on modulation of signaling via individual members of the D_2-class receptors was not within the scope of the present study.

D_2-like DRs are thought to be expressed by a subset (~50–60%) of striatal medium spiny neurons (Gerfen, 1992; Surmeier et al., 1996). In accordance with this idea, the fraction of RGS9-null striatal neurons that showed >25% inhibition of glutamate-elicited currents was 0.5 at 1 μM quinpirole, a concentration of quinpirole that is specific for D_2-like DRs. All of the RGS9-null cells responded to 100 μM quinpirole, possibly because of nonspecific effects at this quinpirole concentration. Alternatively, the absence of RGS9 might allow for the functional detection of low levels of D_2-class receptors that are ordinarily not detected. This suggestion is supported by a recent study by Aizman and colleagues, which found that virtually all striatal neurons, both *in vitro* and *in vivo*, contained dopamine receptors of both classes (Aizman et al., 2000).

The relationship between the abnormal electrophysiology in the striatal neurons from the RGS9 knock-out mice and the abnormal behavior detected after dopamine depletion or neuroleptic treatment remains to be elucidated. Unfortunately, electrophysiological recordings in mutant mice were successful only in animals younger than 4 weeks. Thus, all electrophysiological data were taken in animals that were not weaned and hence were too young to reproduce the behavioral abnormalities that we detected in older animals. However, these data are a first step toward understanding the cellular mechanisms for the locomotor abnormalities observed in the older RGS9-null mice.

A model for dyskinesias?

There are few animal models for drug-induced dyskinesias (Kulkarni and Naidu, 2001), and the abnormal involuntary movements described in this study (Fig. 1) more closely resemble drug-induced dyskinesia in humans than other reported rodent models such as vacuous chewing (Andreassen et al., 2001).

Direct treatment of the knock-out mice with D_2DR agonists only produced minor increases in locomotion. Disorders similar to the drug-induced dyskinesias were produced exclusively in RGS9 knock-out mice and only when D_2DR agonist treatment was preceded by a prolonged inhibition of dopaminergic transmission (see Materials and Methods). There is evidence that chronic inhibition of dopamine signaling along the nigrostriatal dopamine pathway can produce D_2DR supersensitivity (i.e., enhanced cellular signaling) that may result from an increase in the number of striatal D_2DR (Rubinstein et al., 1990; LaHoste and Marshall, 1994).

RGS9-2 could suppress these abnormal movements via either of two mechanisms. By accelerating the termination of G-protein signals, RGS proteins attenuate the integrated cellular effects of G-protein activation (Ross and Wilkie, 2000). RGS9-2 and D_2DR are found coexpressed in striatal medium spiny neurons (Rahman et al., 2003), and RGS9-2 can accelerate the termination of D_2DR signals (Fig. 5*E*,*F*). Because RGS9-2 is targeted to D_2DR via the RGS9-2 DEP domain, it is well situated to influence any functional effects of altered D_2DR expression that may result from prolonged antipsychotic treatment (Rubinstein et al., 1990; LaHoste and Marshall, 1994). Thus, drugs targeting RGS9-2 might be useful in the treatment of dyskinesias (Neubig and Siderovski, 2002).

Alternatively, the RGS9 DEP domain in conjunction with other proteins may compartmentalize D_2-like DRs so as to prevent D_2-like DR-mediated inhibition of NMDA-elicited conductances. Prolonged inhibition of dopaminergic signaling could alter expression levels of either D_2DR or RGS9-2 so as to disrupt

such compartmentalization, leading to an abnormal signaling and abnormal involuntary movements.

In our RGS9 knock-out mouse model, we elicited abnormal movements after only 3 d of drug treatment. Dyskinesias in human patients occur only after months, if not years, of therapy and may reflect the time required for significant alterations in striatal D_2DR or RGS9-2. The speedier onset of abnormal movements in the RGS9 knock-out mice may result from the complete loss of RGS9-2 expression resulting from the genetic ablation of RGS9. If dysregulation of RGS9 contributes to drug-induced dyskinesia in humans, alterations are presumably more subtle and require time to develop.

References

Aizman O, Brismar H, Uhlen P, Zettergren E, Levey AI, Forssberg H, Greengard P, Aperia A (2000) Anatomical and physiological evidence for D1 and D2 dopamine receptor colocalization in neostriatal neurons. Nat Neurosci 3:226–230.

Andreassen OA, Meshul CK, Moore C, Jorgensen HA (2001) Oral dyskinesias and morphological changes in rat striatum during long-term haloperidol administration. Psychopharmacology (Berl) 157:11–19.

Berman DM, Gilman AG (1998) Mammalian RGS proteins: barbarians at the gate. J Biol Chem 273:1269–1272.

Bibbiani F, Kielaite A, Chase TN (2004) Effect of the simultaneous blockade of AMPA and NMDA receptors on levodopa-induced dyskinesias in MPTP-lesioned primates. In: 8th International Congress of Parkinson's Disease and Movement Disorders (Goetz CG, Deuschl G, eds), pp A257–A258. Rome: The Movement Disorder Society.

Blackwell KT, Czubayko U, Plenz D (2003) Quantitative estimate of synaptic inputs to striatal neurons during up and down states *in vitro*. J Neurosci 23:9123–9132.

Cabrera-Vera TM, Hernandez S, Earls LR, Medkova M, Sundgren-Andersson AK, Surmeier DJ, Hamm HE (2004) RGS9-2 modulates D2 dopamine receptor-mediated Ca^{2+} channel inhibition in rat striatal cholinergic interneurons. Proc Natl Acad Sci USA 101:16339–16344.

Cenci MA, Whishaw IQ, Schallert T (2002) Animal models of neurological deficits: how relevant is the rat? Nat Rev Neurosci 3:574–579.

Centonze D, Grande C, Saulle E, Martin AB, Gubellini P, Pavon N, Pisani A, Bernardi G, Moratalla R, Calabresi P (2003) Distinct roles of D_1 and D_5 dopamine receptors in motor activity and striatal synaptic plasticity. J Neurosci 23:8506–8512.

Chen CK, Burns ME, He W, Wensel TG, Baylor DA, Simon MI (2000) Slowed recovery of rod photoresponse in mice lacking the GTPase accelerating protein RGS9-1. Nature 403:557–560.

Dascal N (2001) Ion-channel regulation by G proteins. Trends Endocrinol Metab 12:391–398.

Dauer W, Przedborski S (2003) Parkinson's disease: mechanisms and models. Neuron 39:889–909.

De Vries L, Gist Farquhar M (1999) RGS proteins: more than just GAPs for heterotrimeric G proteins. Trends Cell Biol 9:138–144.

De Vries L, Zheng B, Fischer T, Elenko E, Farquhar MG (2000) The regulator of G protein signaling family. Annu Rev Pharmacol Toxicol 40:235–271.

Doupnik CA, Davidson N, Lester HA, Kofuji P (1997) RGS proteins reconstitute the rapid gating kinetics of $G_{\beta\gamma}$-activated inwardly rectifying K^+ channels. Proc Natl Acad Sci USA 94:10461–10466.

Druey KM (2001) Bridging with GAPs: receptor communication through RGS proteins. Sci STKE 2001:RE14.

Dunah AW, Wang Y, Yasuda RP, Kameyama K, Huganir RL, Wolfe BB, Standaert DG (2000) Alterations in subunit expression, composition, and phosphorylation of striatal *N*-methyl-D-aspartate glutamate receptors in a rat 6-hydroxydopamine model of Parkinson's disease. Mol Pharmacol 57:342–352.

Freedman R (2003) Schizophrenia. N Engl J Med 349:1738–1749.

Gerfen CR (1992) The neostriatal mosaic: multiple levels of compartmental organization. Trends Neurosci 15:133–139.

Kawaguchi Y, Wilson CJ, Emson PC (1990) Projection subtypes of rat neostriatal matrix cells revealed by intracellular injection of biocytin. J Neurosci 10:3421–3438.

Kovoor A, Chen CK, He W, Wensel TG, Simon MI, Lester HA (2000) Coexpression of Gbeta5 enhances the function of two Ggamma subunit-like domain-containing regulators of G protein signaling proteins. J Biol Chem 275:3397–3402.

Kulkarni SK, Naidu PS (2001) Animal models of tardive dyskinesia–a review. Indian J Physiol Pharmacol 45:148–160.

LaHoste GJ, Marshall JF (1994) Rapid development of D1 and D2 dopamine receptor supersensitivity as indicated by striatal and pallidal Fos expression. Neurosci Lett 179:153–156.

LaHoste GJ, Wigal T, King BH, Schuck SE, Crinella FM, Swanson JM (2000) Carbamazepine reduces dopamine-mediated behavior in chronic neuroleptic-treated and untreated rats: implications for treatment of tardive dyskinesia and hyperdopaminergic states. Exp Clin Psychopharmacol 8:125–132.

Lundblad M, Andersson M, Winkler C, Kirik D, Wierup N, Cenci MA (2002) Pharmacological validation of behavioural measures of akinesia and dyskinesia in a rat model of Parkinson's disease. Eur J Neurosci 15:120–132.

Missale C, Nash SR, Robinson SW, Jaber M, Caron MG (1998) Dopamine receptors: from structure to function. Physiol Rev 78:189-225.

Neubig RR, Siderovski DP (2002) Regulators of G-protein signalling as new central nervous system drug targets. Nat Rev Drug Discov 1:187–197.

Nicola SM, Surmeier J, Malenka RC (2000) Dopaminergic modulation of neuronal excitability in the striatum and nucleus accumbens. Annu Rev Neurosci 23:185–215.

Ponting CP, Bork P (1996) Pleckstrin's repeat performance: a novel domain in G-protein signaling? Trends Biochem Sci 21:245–246.

Prou D, Gu WJ, Le Crom S, Vincent JD, Salamero J, Vernier P (2001) Intracellular retention of the two isoforms of the D(2) dopamine receptor promotes endoplasmic reticulum disruption. J Cell Sci 114:3517–3527.

Rahman Z, Gold SJ, Potenza MN, Cowan CW, Ni YG, He W, Wensel TG, Nestler EJ (1999) Cloning and characterization of RGS9-2: a striatal-enriched alternatively spliced product of the RGS9 gene. J Neurosci 19:2016–2026.

Rahman Z, Schwarz J, Gold SJ, Zachariou V, Wein MN, Choi KH, Kovoor A, Chen CK, DiLeone RJ, Schwarz SC, Selley DE, Sim-Selley LJ, Barrot M, Luedtke RR, Self D, Neve RL, Lester HA, Simon MI, Nestler EJ (2003) RGS9 modulates dopamine signaling in the basal ganglia. Neuron 38:941–952.

Rascol O, Fabre N (2001) Dyskinesia: L-DOPA-induced and tardive dyskinesia. Clin Neuropharmacol 24:313–323.

Ross EM, Wilkie TM (2000) GTPase-activating proteins for heterotrimeric G proteins: regulators of G protein signaling (RGS) and RGS-like proteins. Annu Rev Biochem 69:795–827.

Rubinstein M, Muschietti JP, Gershanik O, Flawia MM, Stefano FJ (1990) Adaptive mechanisms of striatal D1 and D2 dopamine receptors in response to a prolonged reserpine treatment in mice. J Pharmacol Exp Ther 252:810–816.

Sawa A, Snyder SH (2002) Schizophrenia: diverse approaches to a complex disease. Science 296:692–695.

Surmeier DJ, Song WJ, Yan Z (1996) Coordinated expression of dopamine receptors in neostriatal medium spiny neurons. J Neurosci 16:6579–6591.

Thomas EA, Danielson PE, Sutcliffe JG (1998) RGS9: a regulator of G-protein signalling with specific expression in rat and mouse striatum. J Neurosci Res 52:118–124.